The Generalized Scattering Matrix of Closely Spaced Strip and Slot Layers in Waveguide

Alexander B. Yakovlev, *Member, IEEE*, Ahmed I. Khalil, *Student Member, IEEE*,
Chris W. Hicks, *Student Member, IEEE*, Amir Mortazawi, *Member, IEEE*, and Michael B. Steer, *Fellow, IEEE*

Abstract—In this paper, a method-of-moments integral-equation formulation of a generalized scattering matrix (GSM) is presented for the full-wave analysis of interactive planar electric and magnetic discontinuities in waveguide. This was developed to efficiently handle a variety of waveguide-based strip-to-slot transitions, especially on thin substrates. This single matrix formulation replaces the problematic procedure of cascading individual GSM's of an electric (strip) layer, a thin substrate, and a magnetic (slot) layer.

Index Terms—Electromagnetic analysis, generalized scattering matrix, Green's functions, method of moments, patch, slot antennas, waveguide transition.

I. INTRODUCTION

MANY waveguide-based microwave and millimeter-wave systems are constructed as cascaded blocks. For example, some waveguide-based filters and spatial power combiners consist of a number of transverse patterned conductive layers separated by waveguide sections, as shown in Fig. 1. This structure can be modeled as five blocks: one for each of the three waveguide sections of permittivity ϵ_1, ϵ_2, and ϵ_3, one for the layer containing the metal strip at $z = 0$, and the other for the layer containing the slot at $z = \tau$. It would be possible to electromagnetically characterize this structure using a multilayer method-of-moments (MoM) technique in which the conductors are discretized. Such discretization can result in a very large matrix problem. Also, this approach cannot be used when a block requires three-dimensional (3-D) electromagnetic (EM) characterization obtained, for example, using the FEM. A solution is to use the generalized scattering matrix (GSM) procedure, in which the field in the waveguide is decomposed into a number of orthogonal waveguide modes. An EM analysis of one block at a time then enables the coefficients of the forward and backward traveling components at each of the two internal waveguide surfaces of a block to be related. The GSM's of each block can then be cascaded to obtain the overall system characterization. The GSM has two attributes that are important for system design. The first is that it uses memory efficiently as the memory is determined by the
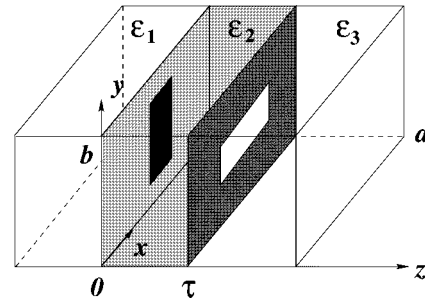
A. B. Yakovlev, A. I. Khalil, C. W. Hicks, and A. Mortazawi are with the Electrical and Computer Engineering Department, North Carolina State University, Raleigh, NC 27695-7914 USA (e-mail: yakovlev@ieee.org).

M. B. Steer is with the Institute of Microwaves and Photonics, School of Electronic and Electrical Engineering, The University of Leeds, Leeds LS2 9JT, U.K. (e-mail: m.b.steer@ieee.org).

Publisher Item Identifier S 0018-9480(00)00225-8.

Fig. 1. Geometry of a rectangular waveguide-based strip-to-slot transition module: strip is 0.6 mm × 5.4 mm, slot is 5.4 mm × 0.6 mm, $a = 22.86$ mm, $b = 10.16$ mm, $\tau = 2.5$ mm, $\epsilon_1 = 1.0$, $\epsilon_2 = 6.0$, $\epsilon_3 = 1.0$.

discretization of a single block rather than the discretization of the whole system. The memory required to represent the GSM of each block is determined by the number of waveguide modes required to represent the field adequately. With the appropriate choice of blocks, this is relatively small. The second is that, in an iterative design procedure, some blocks will be unchanged, and the EM characterization of these can be reused.

The work reported in this paper was developed for the modeling of waveguide-based spatial power-combining systems [1], [2]. Spatial power-combining systems generally consist of an array of unit cell amplifiers arranged in a regular two-dimensional array. A GSM approach in conjunction with MoM discretization was developed in [3] for the analysis of quasi-optical grids used for grid amplifiers and grid oscillators. Active device ports are incorporated in the algorithm in terms of normalized Floquet harmonics that allows polarizers and periodic grid structures to be modeled without the need of ideal magnetic and electric walls. A full-wave analysis of infinite periodic grid structures with active devices was proposed in [4] based on the MoM solution for the electric current density discretized by rooftop basis functions on the grid surface. The algorithm was implemented for a single unit cell of the infinite grid using specific approximations (equiphase conditions with the introduction of electric and magnetic walls). Three-dimensional finite-difference time-domain analysis of infinite periodic grid structures was presented in [5] using Floquet boundary conditions and Berenger's perfectly matched layer absorbing boundary condition. The technique was used to model a multilayer quasi-optical rotator array and compared with measurements. The problem with the above techniques are that idealized conditions are assumed, particularly infinite periodicity. A novel MoM-based GSM modeling scheme was recently proposed by the authors for efficient simulation of large waveguide-based
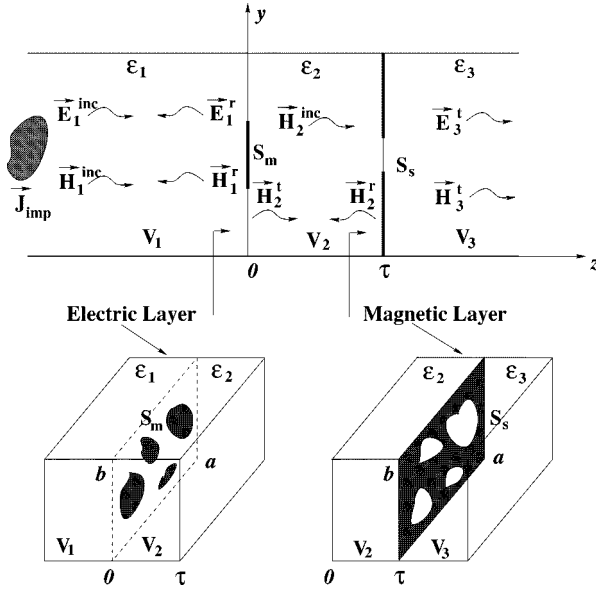
Fig. 2. Geometry of a waveguide-based transition module of arbitrarily shaped interactive electric and magnetic layers.

EM and quasi-optical systems for spatial power combining [6]. The development of field-circuit interfaces to simulate interaction between passive and active [monolithic microwave integrated circuit (MMIC)] devices and circuits is a novel, but necessary, development for integrated EM and circuit modeling. The idea of partitioning a whole system into individual modules (electric or magnetic layer) is implemented and the GSM of each layer is obtained based on a full-wave MoM formulation. Internal ports connecting MMIC devices and passive circuit elements with the distributed structure are established in the technique and these ports are retained in the cascading of blocks. The GSM is constructed for all propagating and evanescent TE and TM modes and provides an accurate simulation of interactions between neighboring modules. A problem occurs when the separation between neighboring layers becomes electrically small. This necessitates a significant increase in the number of waveguide modes (i.e., the size of the GSM) in order to provide the adequate interaction of cascading modules. In turn, this results in a dramatic increase of memory and computational requirements. The solution is to model two closely spaced layers as a single block rather than as the cascade of three blocks. The particular problem addressed here is shown in Fig. 2. The new block consists of the electric layer (the conductors) at $z = 0$, the volume between $z = 0$ and $z = \tau$, and the magnetic layer (the slots) at $z = \tau$. It is the purpose of this paper to develop the GSM formulation for this enlarged block.

In this paper, a full-wave integral-equation formulation is developed for EM modeling of waveguide-based arbitrarily shaped interactive electric (strip, patch) and magnetic (slot, aperture) discontinuities. In essence, the MoM-based GSM formulation is developed for two close layers, which are then modeled as a single block. The incident electric and magnetic fields are expressed in terms of eigenmode expansions with unknown magnitudes, including both propagating and evanescent TE and TM modes normalized by a unity power condition

[7]. A coupled set of the electric- and magnetic-field integral equations is discretized via the MoM using piecewise-sinusoidal overlapping basis and testing functions for the electric and magnetic current density. The MoM matrix equation yields a matrix representation for the electric and magnetic current amplitude coefficients in terms of the unknown magnitudes of incident electric and magnetic fields expressed in terms of waveguide modes (eigenmode expansions) and the inverse MoM matrix. The magnitudes of scattered (reflected and transmitted) modes are obtained in terms of current amplitude coefficients using a unity power normalization for the electric and magnetic vector functions. Finally, this procedure results in the GSM representation relating magnitudes of incident and scattered modes. The method is numerically stable for thin as well as thick substrates and requires the same central processing unit (CPU) time and computer memory for each separation between the electric and magnetic layers (in the range from micrometers to centimeters and larger). Numerical results are obtained for various waveguide-based interactive electric and magnetic layers and compared with measurement data and data obtained using a GSM cascading modeling scheme from [6] (for electrically large separation between layers) and a 3-D commercial FEM program.

II. INTEGRAL-EQUATION FORMULATION AND GENERALIZED SCATTERING MATRIX METHOD

A. Introduction

Consider a waveguide-based transition module with three dielectric layers, as shown in Fig. 2. An arbitrarily shaped metallization S_m (electric layer) and slot apertures S_s in a ground plane (magnetic layer) are located on the interfaces of adjacent dielectric layers with permittivities ϵ_1 and ϵ_2, and ϵ_2 and ϵ_3, respectively. The incident electric and magnetic fields in the region V_1 are generated by an impressed electric current source $\overline{\boldsymbol{J}}_{\mathrm{imp}}$ ($\nabla \times \overline{\boldsymbol{J}}_{\mathrm{imp}}$ for the magnetic field). It should be noted that an incident magnetic field from region V_3 is similarly handled. The scattered electric and magnetic fields in the regions V_1 and V_2 are generated by the induced electric current on the metallization S_m and by the induced magnetic current on the surface of slot apertures S_s (note that both electric and magnetic currents contribute to the fields). The electric and magnetic fields in the region V_3 are due to magnetic currents only, but the continuity of tangential components of the magnetic field across the surface S_s provides the interaction of all regions and necessitates the formulation of the problem in terms of coupled electric- and magnetic-field integral equations.

B. Electric and Magnetic Layers

A coupled set of integral equations is obtained by enforcing a boundary condition on the tangential components of the electric field on the conducting surface S_m at $z = 0$ as follows:

$$\hat{z} \times \left(\overline{\boldsymbol{E}}_1^{\mathrm{inc}}(\vec{r}) + \overline{\boldsymbol{E}}_1^{\mathrm{scat}}(\vec{r}) \right) = 0 \qquad (1)$$

and a continuity condition on the tangential components of the magnetic field on the surface of the slot apertures S_s at $z = \tau$ as follows:

$$\hat{z} \times \left(\overline{\boldsymbol{H}}_2^{\text{inc}}(\vec{r}) + \overline{\boldsymbol{H}}_2^{\text{scat}}(\vec{r}) \right) = \hat{z} \times \overline{\boldsymbol{H}}_3^{\text{scat}}(\vec{r}) \qquad (2)$$

where $\overline{\boldsymbol{E}}_1^{\text{scat}}(\vec{r})$, $\overline{\boldsymbol{H}}_2^{\text{scat}}(\vec{r})$, and $\overline{\boldsymbol{H}}_3^{\text{scat}}(\vec{r})$ are scattered electric and magnetic fields. Note that $\overline{\boldsymbol{H}}_2^{\text{inc}}(\vec{r})$ is a part of the incident magnetic field transmitted from the region V_1 through the dielectric interface at $z = 0$.

The integral form of the boundary condition (1) is obtained by combining the vector-wave equation formulation for the electric field and the corresponding formulation for the electric dyadic Green's function. The integral-equation formulation of the second vector-dyadic Green's theorem [8] with appropriate boundary and continuity conditions is

$$- \jmath\omega\mu_0 \hat{z} \times \int_{V_{\text{imp}}} \overline{\boldsymbol{J}}_{\text{imp}}(\vec{r}') \cdot \overline{\overline{\boldsymbol{G}}}_{e1}^{(11)}(\vec{r}', \vec{r}) \, dV'$$

$$= \jmath\omega\mu_0 \hat{z} \times \int_{S_m} \overline{\boldsymbol{J}}(\vec{r}') \cdot \overline{\overline{\boldsymbol{G}}}_{e1}^{(11)}(\vec{r}', \vec{r}) \, dS'$$

$$- \hat{z} \times \int_{S_s} \overline{\boldsymbol{M}}(\vec{r}') \cdot \left[\nabla' \times \overline{\overline{\boldsymbol{G}}}_{e1}^{(21)}(\vec{r}', \vec{r}) \right] dS'. \qquad (3)$$

Here, the integral on the left-hand side of (3) represents the incident electric field due to impressed electric current $\overline{\boldsymbol{J}}_{\text{imp}}(\vec{r}')$ and the integrals on the right-hand side are the scattered electric fields due to induced electric $\overline{\boldsymbol{J}}(\vec{r}')$ and magnetic $\overline{\boldsymbol{M}}(\vec{r}')$ currents. The electric dyadic Green's functions $\overline{\overline{\boldsymbol{G}}}_{e1}^{(11)}(\vec{r}, \vec{r}')$ and $\overline{\overline{\boldsymbol{G}}}_{e1}^{(21)}(\vec{r}, \vec{r}')$ are obtained as the solution of the boundary-value problem for a semiinfinite two-layered waveguide terminated by a ground plane at $z = \tau$ (similar formulations for electric Green's dyadics are presented in [8]). The electric dyadic Green's functions satisfy boundary and continuity conditions for the electric-field vector on the surface of a conducting shield and on the interface of adjacent dielectric layers with permittivities ϵ_1 and ϵ_2. The formulation of the boundary-value problem for the electric Green's dyadics and some analytical details are provided in Appendix A.

The continuity condition for tangential components of the magnetic field (2) is obtained in integral form using a similar procedure as that described above for the electric-field vector resulting in the magnetic-field integral equation for the unknown currents $\overline{\boldsymbol{J}}(\vec{r}')$ and $\overline{\boldsymbol{M}}(\vec{r}')$ as follows:

$$\frac{\epsilon_2}{\epsilon_1} \hat{z} \times \int_{V_{\text{imp}}} \left[\nabla' \times \overline{\boldsymbol{J}}_{\text{imp}}(\vec{r}') \right] \cdot \overline{\overline{\boldsymbol{G}}}_{e2}^{(12)}(\vec{r}', \vec{r}) \, dV'$$

$$= - \frac{\epsilon_2}{\epsilon_1} \hat{z} \times \int_{S_m} \overline{\boldsymbol{J}}(\vec{r}') \cdot \left[\nabla' \times \overline{\overline{\boldsymbol{G}}}_{e2}^{(12)}(\vec{r}', \vec{r}) \right] dS'$$

$$- \jmath\omega\epsilon_0 \hat{z} \times \int_{S_s} \overline{\boldsymbol{M}}(\vec{r}')$$

$$\cdot \left[\epsilon_2 \overline{\overline{\boldsymbol{G}}}_{e2}^{(22)}(\vec{r}', \vec{r}) + \epsilon_3 \overline{\overline{\boldsymbol{G}}}_{e2}^{(3)}(\vec{r}', \vec{r}) \right] dS'. \qquad (4)$$

The integral on the left-hand side of (4) represents the incident magnetic field introduced in the region V_2 and the integrals on the right-hand side are the scattered magnetic fields due

to induced electric $\overline{\boldsymbol{J}}(\vec{r}')$ and magnetic $\overline{\boldsymbol{M}}(\vec{r}')$ currents. The electric dyadic Green's functions $\overline{\overline{\boldsymbol{G}}}_{e2}^{(12)}(\vec{r}, \vec{r}')$, $\overline{\overline{\boldsymbol{G}}}_{e2}^{(22)}(\vec{r}, \vec{r}')$ have been derived for semiinfinite two-layer waveguide satisfying boundary and continuity conditions for the magnetic field vector (see the formulation in Appendix B). The electric dyadic Green's function of the second kind $\overline{\overline{\boldsymbol{G}}}_{e2}^{(3)}(\vec{r}, \vec{r}')$ is obtained for a single-layered semiinfinite waveguide terminated by a ground plane at $z = \tau$ (details are given in Appendix C). Green's functions in this formulation are obtained in terms of double series expansions over the complete system of eigenfunctions of the Helmholtz operator. Dyadic Green's functions in terms of rectangular vector-wave functions have also been constructed for a semiinfinite rectangular waveguide with multilayered loading [9].

The incident electric and magnetic fields introduced in integral form in (3) and (4) are determined at the point of observation $\vec{r}$ due to current sources $\overline{\boldsymbol{J}}_{\text{imp}}(\vec{r}')$ and $\nabla' \times \overline{\boldsymbol{J}}_{\text{imp}}(\vec{r}')$ at the source point $\vec{r}'$. This representation naturally comes from the integral-equation formulation using the second vector-dyadic Green's theorem, but at the same time, it requires an explicit form for the electric current source. An alternative to the integral representation, a series eigenmode expansion, including both propagating and evanescent TE and TM modes, is proposed here. The total incident electric field introduced by the boundary condition (1) at $z = 0$ is given as

$$\overline{\boldsymbol{E}}_1^{\text{inc}}(\vec{r}) = \sum_{m=0}^{\infty} \sum_{m \neq n = 0}^{\infty} a_{mn}^{\text{TE}} \overline{\boldsymbol{e}}_{mn}^{+\text{TE}}(x, y) \left(1 + R_{mn}^{\text{TE}} \right)$$

$$+ \sum_{m=1}^{\infty} \sum_{n=1}^{\infty} a_{mn}^{\text{TM}} \overline{\boldsymbol{e}}_{mn}^{+\text{TM}}(x, y) \left(1 + R_{mn}^{\text{TM}} \right). \qquad (5)$$

The total incident magnetic field that appears in the continuity condition (2) at $z = \tau$ is determined similarly as

$$\overline{\boldsymbol{H}}_2^{\text{inc}}(\vec{r}) = \sum_{m=0}^{\infty} \sum_{m \neq n = 0}^{\infty} 2a_{mn}^{\text{TE}} T_{mn}^{\text{TE}} \overline{\boldsymbol{h}}_{mn}^{+\text{TE}}(x, y) e^{-\gamma_{mn}^{(2)}\tau}$$

$$+ \sum_{m=1}^{\infty} \sum_{n=1}^{\infty} 2a_{mn}^{\text{TM}} T_{mn}^{\text{TM}} \overline{\boldsymbol{h}}_{mn}^{+\text{TM}}(x, y) e^{-\gamma_{mn}^{(2)}\tau} \qquad (6)$$

where a_{mn}^{TE}, a_{mn}^{TM} are unknown magnitudes of all propagating and evanescent TE and TM modes, respectively, and $\gamma_{mn}^{(i)}$, $(i = 1, 2)$ is the propagation constant defined as

$$\gamma_{mn}^{(i)} = \begin{cases} \jmath\sqrt{k_i^2 - k_c^2}, & k_i^2 > k_c^2 \\ \sqrt{k_c^2 - k_i^2}, & k_i^2 < k_c^2 \end{cases}$$

and

$$k_c^2 = k_x^2 + k_y^2 \quad k_x = \frac{m\pi}{a} \quad k_y = \frac{n\pi}{b} \quad k_i = \frac{2\pi}{\lambda_0}\sqrt{\epsilon_i}. \qquad (7)$$

The vector functions $\overline{\boldsymbol{e}}_{mn}(x, y)$ and $\overline{\boldsymbol{h}}_{mn}(x, y)$ introduced in (5) and (6) for the electric and magnetic fields of TE and TM

modes, respectively, satisfy the unity power normalization condition [7]

$$\int_{S_w} \left[\overline{e}_{mn}^{\pm}(x, y) \times \overline{h}_{mn}^{\pm}(x, y) \right] \cdot (\pm \hat{z})\, dS = 1. \qquad (8)$$

Here, the "$\pm$" sign corresponds to waves propagating in the positive (+) and negative (−) z-directions and S_w is the waveguide cross section. The expressions for the electric and magnetic vector function components for TE and TM modes have been derived using the procedure described in [7].

The total reflection R_{mn} and transmission T_{mn} coefficients for TE and TM modes at $z = 0$ are determined as the solution of the boundary-value problem for a two-layered waveguide terminated by a ground plane at $z = \tau$ in the absence of electric and magnetic currents (no strip metallization and slot apertures). Note that the induced electric and magnetic currents in the above formulation are due to total incident electric and magnetic fields that include direct and reflected (transmitted) parts associated only with incident fields. The problems of determining total reflection and transmission coefficients have been solved separately for TE and TM modes by matching continuity conditions on the dielectric interface at $z = 0$ and boundary conditions at $z = \tau$

$$R_{mn}^{\text{TE, TM}} = \frac{R_{12}^{\text{TE, TM}} - e^{-2\gamma_{mn}^{(2)}\tau}}{1 - R_{12}^{\text{TE, TM}} e^{-2\gamma_{mn}^{(2)}\tau}}$$

$$T_{mn}^{\text{TE, TM}} = \frac{T_{12}^{\text{TE, TM}}}{1 - R_{12}^{\text{TE, TM}} e^{-2\gamma_{mn}^{(2)}\tau}}$$

where

$$R_{12}^{\text{TE}} = \frac{\gamma_{mn}^{(1)} - \gamma_{mn}^{(2)}}{\gamma_{mn}^{(1)} + \gamma_{mn}^{(2)}}$$

$$T_{12}^{\text{TE}} = \frac{2\sqrt{\gamma_{mn}^{(1)}\gamma_{mn}^{(2)}}}{\gamma_{mn}^{(1)} + \gamma_{mn}^{(2)}}$$

$$R_{12}^{\text{TM}} = \frac{\epsilon_1 \gamma_{mn}^{(2)} - \epsilon_2 \gamma_{mn}^{(1)}}{\epsilon_1 \gamma_{mn}^{(2)} + \epsilon_2 \gamma_{mn}^{(1)}}$$

$$T_{12}^{\text{TM}} = \frac{2\sqrt{\epsilon_1 \gamma_{mn}^{(2)} \epsilon_2 \gamma_{mn}^{(1)}}}{\epsilon_1 \gamma_{mn}^{(2)} + \epsilon_2 \gamma_{mn}^{(1)}}. \qquad (9)$$

The coupled set of integral equations (3) and (4) with the incident electric and magnetic fields expressed in terms of eigenmode series expansions (5) and (6) is discretized via the traditional MoM using the x- and y-directed overlapping piecewise-sinusoidal basis and testing functions for the electric and magnetic currents

$$J_x(x) = \sum_{i=1}^{N_x} J_i^x W_i^x(x)$$

$$J_y(y) = \sum_{\ell=1}^{N_y} J_\ell^y W_\ell^y(y)$$

$$M_x(x) = \sum_{p=1}^{M_x} M_p^x T_p^x(x)$$

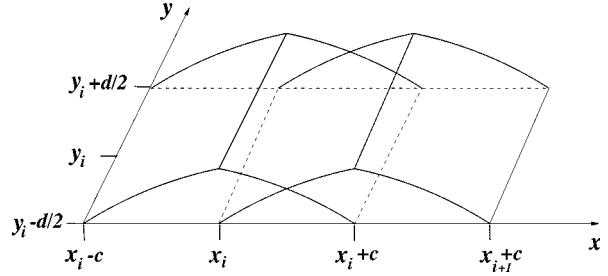$$M_y(y) = \sum_{q=1}^{M_y} M_q^y T_q^y(y). \qquad (10)$$

Fig. 3. Rectangular cells with the x-directed overlapping piecewise-sinusoidal basis functions.

Here, $W_i^x(x)$ are locally determined basis functions defined as

$$W_i^x(x) = \frac{\sin\left[k_s\left(c - |x - x_i|\right)\right]}{d \sin(k_s c)},$$
$$|x - x_i| \le c; \quad |y - y_i| \le d/2$$

and functions $W_\ell^y(y)$, $T_p^x(x)$, and $T_q^y(y)$ have a similar definition. A parameter $k_s = k_0/\sqrt{\epsilon_{\max}}$ determines in some sense a degree of smoothness of the basis functions. Note that these functions are continuous with a discontinuous derivative at $x = x_i$ and, for small $k_s c$, they approach triangular basis functions ($\sin(k_s c) \approx k_s c$). As an example, rectangular cells with the x-directed overlapping basis functions are shown in Fig. 3.

A matrix system of linear equations is obtained for the unknown coefficients in the currents' expansion (10)

$$\boldsymbol{A}\boldsymbol{X} = \boldsymbol{F}^{\text{inc}} \qquad (11)$$

where $\boldsymbol{A}$ is the total MoM matrix of all self and mutual interactions of electric- and magnetic-field components with the electric and magnetic current components

$$\boldsymbol{A} = \begin{bmatrix} \jmath\omega\mu_0 \boldsymbol{Z}(\omega) & \boldsymbol{U}(\omega) \\ \boldsymbol{W}(\omega) & -\jmath\omega\epsilon_0 \boldsymbol{Y}(\omega) \end{bmatrix}$$

$\boldsymbol{X}$ is the vector of unknown currents' coefficients, and $\boldsymbol{F}^{\text{inc}}$ represents tested incident electric and magnetic fields associated with magnitudes a_{mn}

$$\boldsymbol{X} = \begin{bmatrix} \boldsymbol{J} \\ \boldsymbol{M} \end{bmatrix} \qquad \boldsymbol{F}^{\text{inc}} = \begin{bmatrix} \boldsymbol{V} \\ \boldsymbol{I} \end{bmatrix}.$$

The elements of the impedance block matrix $\boldsymbol{Z}(\omega)$ are associated with the electric-field components due to electric current components, obtained in the following integral form at $z = z' = 0$:

$$Z_{ki}^{xx} = \int_{S_m^k} \int_{S_m^i} W_i^x(x') G_{xx,e1}^{(11)}(x', y'; x, y) W_k^x(x)\, dS'\, dS$$

$$Z_{k\ell}^{xy} = \int_{S_m^k} \int_{S_m^\ell} W_\ell^y(y') G_{yx,e1}^{(11)}(x', y'; x, y) W_k^x(x)\, dS'\, dS$$

$$Z_{ji}^{yx} = \int_{S_m^j} \int_{S_m^i} W_i^x(x') G_{xy,e1}^{(11)}(x', y'; x, y) W_j^y(y)\, dS'\, dS$$

$$Z_{j\ell}^{yy} = \int_{S_m^j} \int_{S_m^\ell} W_\ell^y(y') G_{yy,e1}^{(11)}(x', y'; x, y) W_j^y(y)\, dS'\, dS.$$

$$(12)$$

The elements of the block matrix $\boldsymbol{U}(\omega)$ are associated with the electric-field components due to magnetic current components ($z = 0$, $z' = \tau$), shown in (13), at the bottom of this page.

The elements of the block matrix $\boldsymbol{W}(\omega)$ are associated with the magnetic-field components due to electric current components ($z = \tau$, $z' = 0$), shown in (14), at the bottom of this page.

The elements of the admittance block matrix $\boldsymbol{Y}(\omega)$ are associated with the magnetic-field components due to magnetic current components, obtained in the integral form at $z = z' = \tau$, shown in (15), at the bottom of this page.

The electric Green's functions introduced in (12) and (15) have a singularity on the surface of the electric S_m and magnetic S_s layers where a point of observation $\vec{r}$ and a source point $\vec{r}'$ are co-located as a result of the boundary (3) and continuity (4) conditions. This singularity is associated with the primary part of the electric Green's function and it is not integrable in those regions, resulting in a divergent double series of the Green's function expansion. However, the MoM discretization provided in this paper enables a singular integral operator to be partially reduced. The result is that a slowly converging double series [the results of integrating (12) and (15)] is obtained. An acceleration procedure to facilitate a convergence of a double series and speed up the MoM matrix fill is demonstrated in [10] and [11]. An efficient technique to improve a convergence of sincle and double series was also presented in [1616].

The incident electric and magnetic fields (5) and (6) tested with the overlapping piecewise-sinusoidal x- and y-directed functions introduced in (10) can be expressed in matrix form in terms of the unknown magnitudes a_{mn} of the TE and TM modes, as shown in (16)

$$\begin{bmatrix} V \\ I \end{bmatrix} = \boldsymbol{B} \boldsymbol{C} \boldsymbol{a} \tag{16}$$

$$U_{kp}^{xx} = -\int_{S_m^k} \int_{S_s^p} T_p^x(x') \left[\frac{\partial}{\partial y'} G_{zx,e1}^{(21)}(x', y'; x, y) - \frac{\partial}{\partial z'} G_{yx,e1}^{(21)}(x', y'; x, y) \right] W_k^x(x) \, dS' \, dS$$

$$U_{kq}^{xy} = \int_{S_m^k} \int_{S_s^q} T_q^y(y') \left[\frac{\partial}{\partial x'} G_{zx,e1}^{(21)}(x', y'; x, y) - \frac{\partial}{\partial z'} G_{xx,e1}^{(21)}(x', y'; x, y) \right] W_k^x(x) \, dS' \, dS$$

$$U_{jp}^{yx} = -\int_{S_m^j} \int_{S_s^p} T_p^x(x') \left[\frac{\partial}{\partial y'} G_{zy,e1}^{(21)}(x', y'; x, y) - \frac{\partial}{\partial z'} G_{yy,e1}^{(21)}(x', y'; x, y) \right] W_j^y(y) \, dS' \, dS$$

$$U_{jq}^{yy} = \int_{S_m^j} \int_{S_s^q} T_q^y(y') \left[\frac{\partial}{\partial x'} G_{zy,e1}^{(21)}(x', y'; x, y) - \frac{\partial}{\partial z'} G_{xy,e1}^{(21)}(x', y'; x, y) \right] W_j^y(y) \, dS' \, dS. \tag{13}$$

$$W_{ri}^{xx} = -\frac{\epsilon_2}{\epsilon_1} \int_{S_s^r} \int_{S_m^i} W_i^x(x') \left[\frac{\partial}{\partial y'} G_{zx,e2}^{(12)}(x', y'; x, y) - \frac{\partial}{\partial z'} G_{yx,e2}^{(12)}(x', y'; x, y) \right] T_r^x(x) \, dS' \, dS$$

$$W_{r\ell}^{xy} = \frac{\epsilon_2}{\epsilon_1} \int_{S_s^r} \int_{S_m^\ell} W_\ell^y(y') \left[\frac{\partial}{\partial x'} G_{zx,e2}^{(12)}(x', y'; x, y) - \frac{\partial}{\partial z'} G_{xx,e2}^{(12)}(x', y'; x, y) \right] T_r^x(x) \, dS' \, dS$$

$$W_{si}^{yx} = -\frac{\epsilon_2}{\epsilon_1} \int_{S_s^s} \int_{S_m^i} W_i^x(x') \left[\frac{\partial}{\partial y'} G_{zy,e2}^{(12)}(x', y'; x, y) - \frac{\partial}{\partial z'} G_{yy,e2}^{(12)}(x', y'; x, y) \right] T_s^y(y) \, dS' \, dS$$

$$W_{s\ell}^{yy} = \frac{\epsilon_2}{\epsilon_1} \int_{S_s^s} \int_{S_m^\ell} W_\ell^y(y') \left[\frac{\partial}{\partial x'} G_{zy,e2}^{(12)}(x', y'; x, y) - \frac{\partial}{\partial z'} G_{xy,e2}^{(12)}(x', y'; x, y) \right] T_s^y(y) \, dS' \, dS. \tag{14}$$

$$Y_{rp}^{xx} = \int_{S_s^r} \int_{S_s^p} T_p^x(x') \left[\epsilon_2 G_{xx,e2}^{(22)}(x', y'; x, y) + \epsilon_3 G_{xx,e2}^{(3)}(x', y'; x, y) \right] T_r^x(x) \, dS' \, dS$$

$$Y_{rq}^{xy} = \int_{S_s^r} \int_{S_s^q} T_q^y(y') \left[\epsilon_2 G_{yx,e2}^{(22)}(x', y'; x, y) + \epsilon_3 G_{yx,e2}^{(3)}(x', y'; x, y) \right] T_r^x(x) \, dS' \, dS$$

$$Y_{sp}^{yx} = \int_{S_s^s} \int_{S_s^p} T_p^x(x') \left[\epsilon_2 G_{xy,e2}^{(22)}(x', y'; x, y) + \epsilon_3 G_{xy,e2}^{(3)}(x', y'; x, y) \right] T_s^y(y) \, dS' \, dS$$

$$Y_{sq}^{yy} = \int_{S_s^s} \int_{S_s^q} T_q^y(y') \left[\epsilon_2 G_{yy,e2}^{(22)}(x', y'; x, y) + \epsilon_3 G_{yy,e2}^{(3)}(x', y'; x, y) \right] T_s^y(y) \, dS' \, dS. \tag{15}$$

where

$$
B = \begin{bmatrix}
(e_x^{\mathrm{TE}}, W_x) & (e_x^{\mathrm{TM}}, W_x) & 0 & 0 \\
(e_y^{\mathrm{TE}}, W_y) & (e_y^{\mathrm{TM}}, W_y) & 0 & 0 \\
0 & 0 & (h_x^{\mathrm{TE}}, T_x) & (h_x^{\mathrm{TM}}, T_x) \\
0 & 0 & (h_y^{\mathrm{TE}}, T_y) & (h_y^{\mathrm{TM}}, T_y)
\end{bmatrix}
$$

$$
C = \begin{bmatrix}
U + R^{\mathrm{TE}} & 0 \\
0 & U + R^{\mathrm{TM}} \\
T^{\mathrm{TE}} & 0 \\
0 & T^{\mathrm{TM}}
\end{bmatrix}
$$

$$
a = \begin{bmatrix} a^{\mathrm{TE}} \\ a^{\mathrm{TM}} \end{bmatrix}.
$$

Here, (e, W) and (h, T) define the inner product of the vector function components and correspond to the testing functions. R^{TE} and R^{TM} are total reflection coefficients defined in (9), U is the identity matrix, and

$$
T^{\mathrm{TE}} = 2e^{-\gamma_{mn}^{(2)}\tau}T_{mn}^{\mathrm{TE}}, \quad T^{\mathrm{TM}} = 2e^{-\gamma_{mn}^{(2)}\tau}T_{mn}^{\mathrm{TM}}
$$

with T_{mn}^{TE} and T_{mn}^{TM} being total transmission coefficients (for the incident field only) at $z = 0$, as defined by (9). The above matrix representation (16) leads to a relationship between magnitudes of incident and scattered modes—the GSM.

Using the above matrix transformations, the vector X of magnitudes of electric and magnetic currents can be obtained in terms of the unknown magnitudes of incident TE and TM modes using the following matrix product:

$$
\begin{bmatrix} J \\ M \end{bmatrix} = A^{-1}BCa. \tag{17}
$$

C. Reflection Coefficient

The next step in the determination of the GSM for waveguide-based interactive electric and magnetic layers is to represent the scattered electric field (reflected at $z = 0$) in terms of the eigenmode series expansion and relate it to the integral representation of the scattered electric field due to induced electric and magnetic currents. Following the electric-field integral-equation formulation (3), the reflected electric field at $z = 0$ (interface of adjacent dielectric layers with dielectric permittivities ϵ_1 and ϵ_2) has the form

$$
\begin{aligned}
\overline{E}_1^{\mathrm{ref}}(x, y) &= -\jmath\omega\mu_0 \int_{S_m} \overline{J}(x', y') \cdot \overline{\overline{G}}_{e1}^{(11)}(x', y'; x, y)\, dS' \\
&+ \int_{S_s} \overline{M}(x', y') \cdot \left[\nabla' \times \overline{\overline{G}}_{e1}^{(21)}(x', y'; x, y)\right] dS' \\
&+ \sum_{m=0}^{\infty} \sum_{m\neq n=0}^{\infty} a_{mn}^{\mathrm{TE}} R_{mn}^{\mathrm{TE}} \overline{e}_{mn}^{+\mathrm{TE}}(x, y)
\end{aligned}
$$

$$
+ \sum_{m=1}^{\infty} \sum_{n=1}^{\infty} a_{mn}^{\mathrm{TM}} R_{mn}^{\mathrm{TM}} \overline{e}_{mn}^{+\mathrm{TM}}(x, y). \tag{18}
$$

Note that the reflected part of the total incident field is included in (18). An alternative representation of the reflected electric field is obtained in terms of the eigenmode series expansion with unknown magnitudes of reflected TE and TM modes

$$
\overline{E}_1^{\mathrm{ref}}(x, y) = \sum_{m=0}^{\infty} \sum_{m\neq n=0}^{\infty} b_{mn}^{\mathrm{TE}} \overline{e}_{mn}^{-\mathrm{TE}}(x, y)
$$

$$
+ \sum_{m=1}^{\infty} \sum_{n=1}^{\infty} b_{mn}^{\mathrm{TM}} \overline{e}_{mn}^{-\mathrm{TM}}(x, y). \tag{19}
$$

The unity power normalization condition (8) applied to (18) and (19) enables the magnitudes b_{mn} of reflected TE and TM modes to be expressed in the following form:

$$
\begin{aligned}
& \begin{Bmatrix} b_{mn}^{\mathrm{TE}} \\ b_{mn}^{\mathrm{TM}} \end{Bmatrix} \\
&= -\jmath\omega\mu_0 \int_{S_w} \int_{S_m} \left[\overline{J} \cdot \overline{\overline{G}}_{e1}^{(11)} \times \begin{Bmatrix} \overline{h}_{mn}^{-\mathrm{TE}} \\ \overline{h}_{mn}^{-\mathrm{TM}} \end{Bmatrix}\right] \cdot (-\hat{z})\, dS'\, dS \\
&+ \int_{S_w} \int_{S_s} \left[\overline{M} \cdot \left[\nabla' \times \overline{\overline{G}}_{e1}^{(21)}\right] \times \begin{Bmatrix} \overline{h}_{mn}^{-\mathrm{TE}} \\ \overline{h}_{mn}^{-\mathrm{TM}} \end{Bmatrix}\right] \\
&\cdot (-\hat{z})\, dS'\, dS + \begin{Bmatrix} a_{mn}^{\mathrm{TE}} \\ a_{mn}^{\mathrm{TM}} \end{Bmatrix} \begin{Bmatrix} R_{mn}^{\mathrm{TE}} \\ R_{mn}^{\mathrm{TM}} \end{Bmatrix}. \tag{20}
\end{aligned}
$$

The above system of equations can be written in matrix form relating magnitudes b_{mn} of the reflected TE and TM modes to magnitudes a_{mn} of incident modes using unknown magnitudes of the electric and magnetic currents (details of the integration over S_m, S_s, and S_w are omitted here due to their algebraic simplicity) as follows:

$$
b = D \begin{bmatrix} J \\ M \end{bmatrix} + Ra. \tag{21}
$$

Here, D is a 2×2 block matrix obtained as a result of integration of surface integrals introduced in the system of (20), and R is a diagonal matrix with elements being the total reflection coefficients R_{mn}^{TE} or R_{mn}^{TM} determined in (9).

Substituting the vector of electric and magnetic current magnitudes determined as the matrix product (17) into the matrix equation (21), the matrix relationship of the reflected and incident modes is obtained as follows:

$$
b = S_{11}a
$$

with

$$
S_{11} = DA^{-1}BC + R. \tag{22}
$$

This is the reflection coefficient part of the GSM of the whole structure.

D. Transmission Coefficient

In this section of the paper, we derive the GSM transmission coefficient relating magnitudes of incident and transmitted modes associated with the whole structure. The transmitted electric field due to the magnetic current induced on the surface of slot apertures S_s at $z = \tau$ is obtained in the integral form

$$\overline{E}_3^{\mathrm{tr}}(x, y) = - \int_{S_s} \overline{M}(x', y') \cdot \left[\nabla' \times \overline{\overline{G}}_{e1}^{(3)}(x', y'; x, y) \right] dS' \quad (23)$$

where $\overline{\overline{G}}_{e1}^{(3)}$ is the electric dyadic Green's function of the first kind obtained for a single-layered semiinfinite waveguide terminated by a ground plane at $z = \tau$. This Green's function has been extensively studied by many authors and it is presented, for example, in [7], [8], and [12]. Note that $\nabla' \times \overline{\overline{G}}_{e1}^{(3)}(x', y'; x, y) = \nabla' \times \overline{\overline{G}}_{A1}^{(3)}(x', y'; x, y)$, where $\overline{\overline{G}}_{A1}^{(3)}$ is the vector potential dyadic Green's function of the first kind obtained as a diagonalized dyadic for rectangular cavities and waveguides [13], [14].

The electric field transmitted in the region V_3 is also expressed in terms of the eigenmode series expansion with unknown magnitudes of transmitted TE and TM modes

$$\overline{E}_3^{\mathrm{tr}}(x, y) = \sum_{m=0}^{\infty} \sum_{m \neq n=0}^{\infty} c_{mn}^{\mathrm{TE}} \overline{e}_{mn}^{+\mathrm{TE}}(x, y) + \sum_{m=1}^{\infty} \sum_{n=1}^{\infty} c_{mn}^{\mathrm{TM}} \overline{e}_{mn}^{+\mathrm{TM}}(x, y). \quad (24)$$

Note that the components of vector functions $\overline{e}_{mn}$ are obtained in the region V_3 filled with dielectric of permittivity ϵ_3 (characteristic wave impedances for TE and TM modes are determined in this region).

The unity power normalization condition (8) applied to (23) and (24) results in the expression for the magnitudes of transmitted modes in terms of the induced magnetic current

$$\left\{ \begin{matrix} c_{mn}^{\mathrm{TE}} \\ c_{mn}^{\mathrm{TM}} \end{matrix} \right\} = - \int_{S_w} \int_{S_s} \left[\overline{M} \cdot \left[\nabla' \times \overline{\overline{G}}_{e1}^{(3)} \right] \times \left\{ \begin{matrix} \overline{h}_{mn}^{+\mathrm{TE}} \\ \overline{h}_{mn}^{+\mathrm{TM}} \end{matrix} \right\} \right] \cdot \hat{z} \, dS' \, dS. \quad (25)$$

Following the procedure implemented above for the reflection coefficient S_{11}, a matrix relationship between the transmitted and incident modes is obtained as follows:

$$\mathbf{c} = S_{21} a$$

with
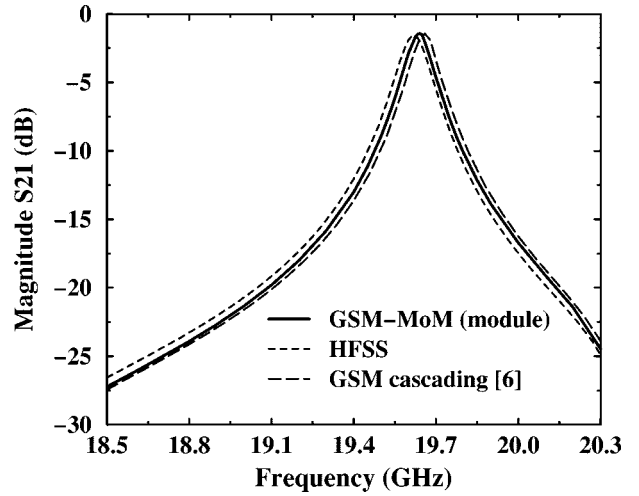
$$S_{21} = LA^{-1}BC. \quad (26)$$

Fig. 4. Magnitude of the transmission coefficient S_{21} against frequency for a strip-to-slot transition module. Numerical results are compared with data obtained using a GSM cascading modeling scheme and a 3-D commercial FEM program.
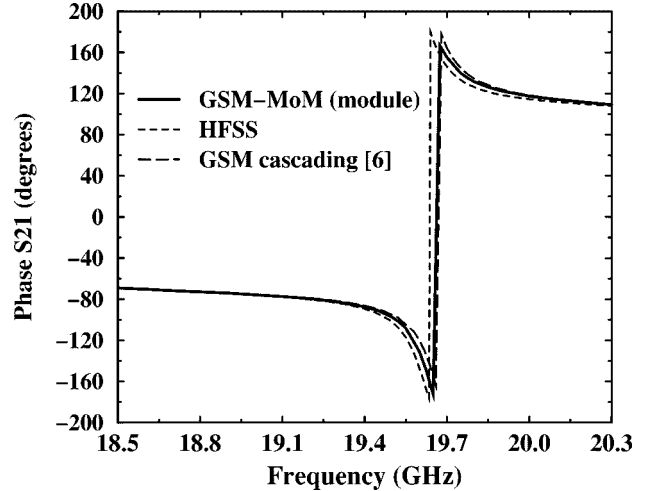

Fig. 5. Phase of the transmission coefficient S_{21} against frequency for a strip-to-slot transition module.

This is the transmission coefficient part of the GSM of the whole structure. The matrix L is analogous to the matrix D and it is constructed in such a way to provide a connection with the matrix product (17). (The electric current is not present in the result (25) and this requires the introduction of zero-element blocks in the matrix L).

The S_{22} and S_{12} coefficients of the GSM are obtained similarly. It should be noted that the integral-equation formulation in conjunction with the GSM method does not require the direct calculation of electric and magnetic currents. Instead, those currents are used to relate magnitudes of scattered (reflected and transmitted) modes to magnitudes of incident modes by means of matrix transformations.

III. NUMERICAL RESULTS AND DISCUSSION

The GSM elements, the reflection and transmission coefficients in (22) and (26), are calculated numerically for a variety of waveguide-based interactive electric and magnetic discontinuities used in EM and quasi-optical power-combining sys-
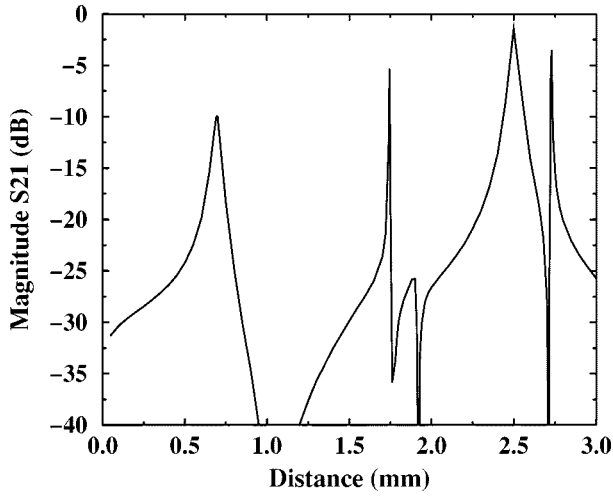
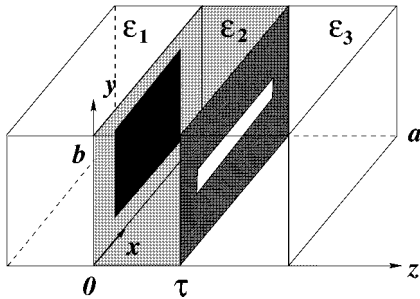Fig. 6. Magnitude of the transmission coefficient S_{21} against separation τ between strip and slot.

Fig. 7. Geometry of a rectangular waveguide-based patch-to-slot transition module: strip is 10.4 mm × 9.0 mm, slot is 10.4 mm × 0.2 mm, $a = 22.86$ mm, $b = 10.16$ mm, $\tau = 0.381$ mm, $\epsilon_1 = 1.0$, $\epsilon_2 = 6.0$, $\epsilon_3 = 1.0$.
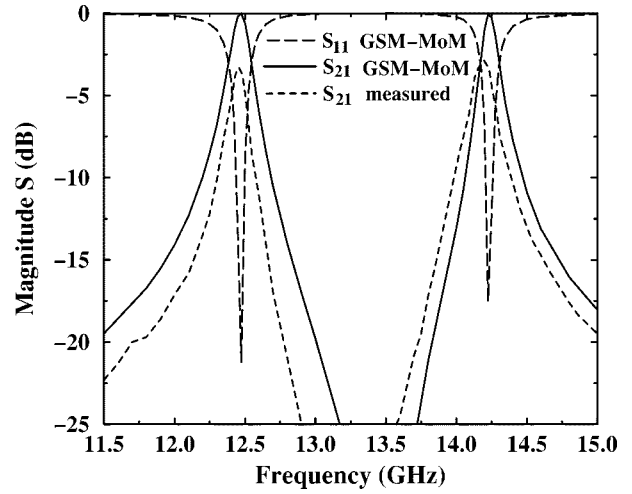

Fig. 8. Magnitude of the reflection S_{11} and transmission S_{21} coefficients against frequency for a resonant patch-to-slot transition. Numerical results are compared with measurement data.
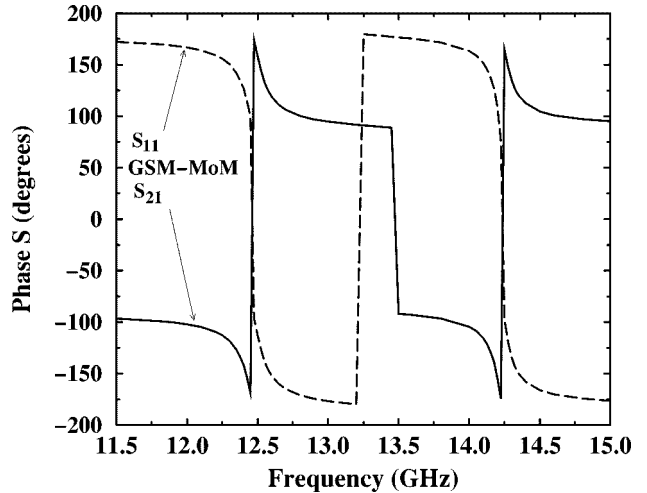

Fig. 9. Phase of the reflection S_{11} and transmission S_{21} coefficients against frequency for a resonant patch-to-slot transition.

tems. In the first example, results are obtained for a waveguide-based rectangular strip-to-slot transition module (Fig. 1) and compared with those generated by the GSM cascading scheme [6] and the commercial HFSS program (Hewlett-Packard, version 5.2). Figs. 4 and 5 demonstrate dispersion characteristics (magnitude and phase) for the transmission S_{21} coefficient in a narrow resonance frequency range (18.5–20.3 GHz) for the dominant TE_{10} mode. Very good agreement of the MoM numerical solution with the GSM cascading and HFSS results is observed. It can be seen that for electrically large substrates ($\tau = 2.5$ mm), the MoM algorithm developed in this paper and the GSM modeling scheme proposed in [6] can both be used to generate the accurate solution for waveguide-based interactive discontinuities.

Note that even though the dispersion behavior of the scattering parameters is shown for the dominant TE_{10} mode, the X-band waveguide in the above frequency range is overmoded and all self and coupling parameters, given by (22) and (26), are calculated. Fig. 6 shows the behavior of the transmission S_{21} coefficient of the TE_{10} mode versus separation τ between the strip metallization and slot aperture. The results are obtained at 19.635 GHz (the resonance frequency from Figs. 4 and 5 for $\tau = 2.5$ mm). It can be seen that the structure resonates at the same frequency for different distances between the strip and slot. The algorithm is numerically stable for different material and geometrical parameters, including thin substrates with

a high dielectric permittivity, and it does not require additional CPU time and memory.

A wide resonant strip (or patch) coupled to a thin slot in a rectangular waveguide with a layered environment is shown in Fig. 7. Numerical results are obtained in the 11.5–15-GHz frequency range for the dominant TE_{10} mode showing a strong patch-to-slot coupling at 12.475 and 14.225 GHz (Fig. 8). Fig. 9 shows the dispersion behavior of the phase of S_{11} and S_{21}, which changes in sign passing through the 0° level at the resonance frequencies. The GSM result for the magnitude of the transmission coefficient S_{21}, shown in Fig. 8, is compared favorably to experiment. The experimental results were obtained using an HP8510C Network Analyzer. The difference observed in peak values of the transmission coefficient is due to conductor loss, dielectric loss, and imperfect connection between the ground plane containing slot at $z = \tau$ and the waveguide walls, which causes a current discontinuity at the edges.

Many spatial power-combining systems are arranged as a multilayer structure with an array of input antennas on one side
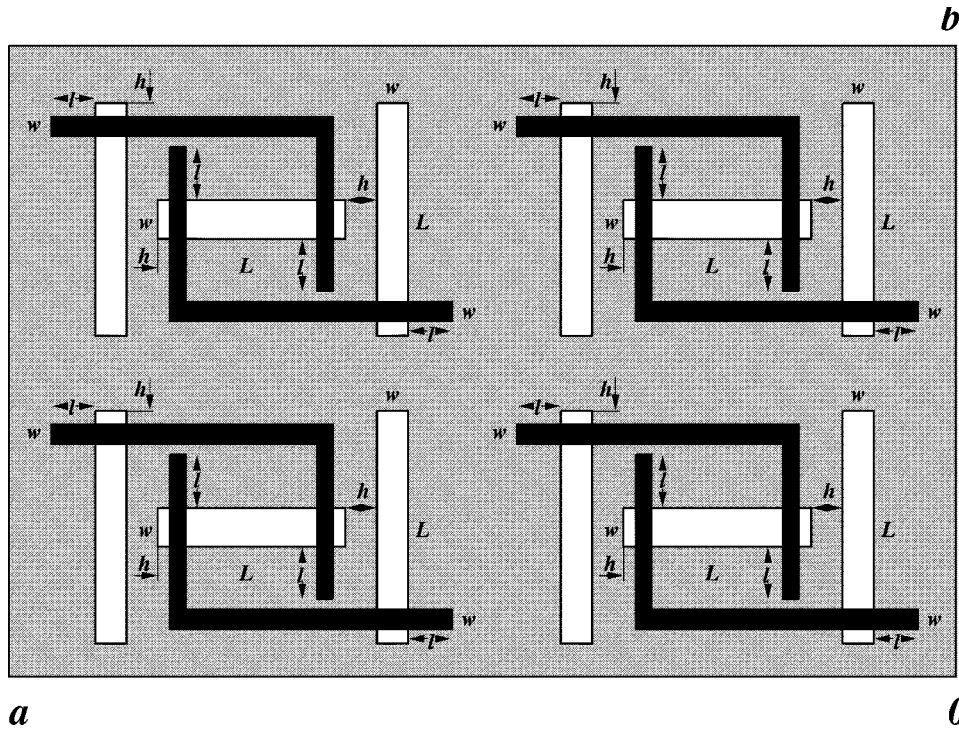
Fig. 10.   Geometry of a waveguide-based cross-polarized 2×2 strip-to-slot array. $a = 7.11$ mm, $b = 3.56$ mm, $L = 1.4$ mm, $w = 0.1$ mm, $l = 0.4$ mm, $h = 0.05$ mm, $\tau = 0.075$ mm, $\epsilon_1 = 2.8$, $\epsilon_2 = 12.9$, $\epsilon_3 = 8.5$.

and an array of output antennas on the other [1], [2]. An active device, a MMIC amplifier, is inserted between an input–output antenna pair. Some structures use an array of coupled slot and strip pairs (Fig. 1) and others use coupled slot and patch antenna structures (Fig. 7). A more complicated structure is shown, in part, in Fig. 10. This structure is a cross-polarized double 2×2 strip-to-slot transition module and is placed in a lateral position across a waveguide. Actual structures could have larger arrangements of 5×5 or more cells. A special property of these structures are that the individual antennas, in this case slots, are subresonant. It is only as an array that the structure has the desired bandpass characteristics and, therefore, it is important to model the array in its entirety. In Fig. 10, and referring to Figs. 1 and 7, the input angled microstrips are located at the interface of dielectric layers with permittivities ϵ_1 (typically air) and ϵ_2. The energy of vertically polarized modes is coupled to the energy of horizontally polarized modes from the input slot antennas (horizontally oriented slots at $z = \tau$) to the output slot antennas (vertically oriented slots also at $z = \tau$) by means of the angled microstrips. At subresonant frequency, input slot antennas are strongly coupled to microstrips designed to couple the energy of vertically polarized modes to the output antennas, which are subresonant for horizontally polarized modes. The input and output slot antennas are located at the interface (ground plane) of dielectric layers with permittivities ϵ_2 and ϵ_3 (again, typically air). Note that the strips and slots are separated by a very thin substrate ($\tau = 0.075$ mm) with a high dielectric permittivity ($\epsilon_2 = 12.9$). The resonant properties of the structure are mostly determined by the resonance frequency of the input slot antenna array. The resonance occurs at frequency 28.15 GHz for this particular geometry enclosed in a layered Ka-band rectangular waveguide. Note that the waveguide is
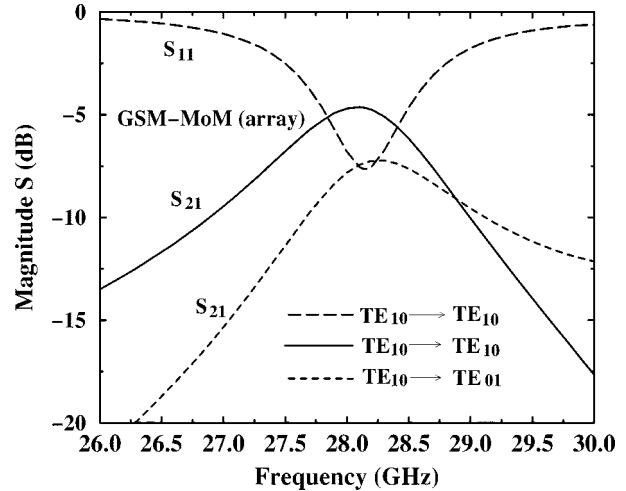

Fig. 11.   Magnitude of the reflection S_{11} and transmission S_{21} coefficients against frequency for the 2×2 waveguide-based strip-to-slot array.

overmoded (even though it operates in the Ka-band frequency range) due to the presence of dielectric layers allowing the higher order modes to propagate. Figs. 11 and 12 show the coupling properties of the transition module: the energy of the TE_{10} mode is transmitted not only through the horizontal input slots (TE_{10} to TE_{10} coupling), but also through the vertical output slots (TE_{10} to TE_{01} coupling), which change the field polarization. When this structure is used in a spatial power-combining system, wherein the input and output signals are separated by vertical and horizontal polarizers, we are particularly interested in providing maximum cross-polarized coupling from the TE_{10} mode to the TE_{01} mode. Note that many modern waveguide-based spatial power-combining
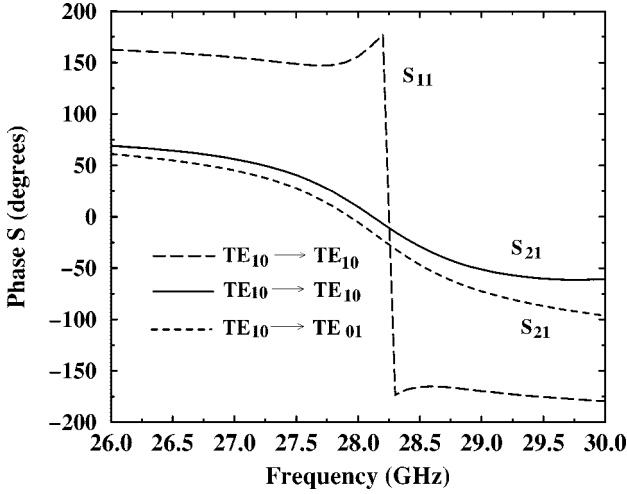
Fig. 12. Phase of the reflection S_{11} and transmission S_{21} coefficients against frequency for the 2×2 waveguide-based strip-to-slot array.

systems are developed with the use of large strip-to-slot (or patch-to-slot) arrays where a strong cross-polarized coupling is provided. The examples demonstrated in this paper show the principles of a waveguide-based cross-polarized coupling, which can be effectively used for the development of large EM and quasi-optical systems.

IV. CONCLUSION

A full-wave integral-equation formulation has been developed for the modeling of waveguide-based, interactive, arbitrarily shaped electric (strip, patch), and magnetic (slot, aperture) layers with application to spatial power-combining systems. The MoM-based GSM algorithm was developed to handle a variety of interactive electric and magnetic disconti-nuities with thin substrates of high dielectric permittivity. The GSM of a transition module is constructed as an individual GSM in the cascading algorithm for the composite GSM of power-combining systems. Numerical results are shown for various waveguide-based transition modules, including strip-to-slot, patch-to-slot, and cross-polarized strip-to-slot array. Modeling of the patch-to-slot and strip-to-slot transitions is also compared with measured data and numerical results generated using a GSM cascading modeling scheme from [6] (for electrically large separation between strip and slot) and a commercial FEM program, respectively. The method is stable for different material and geometrical parameters and can be effectively used for the simulation and analysis of closely spaced interactive discontinuities. These cannot be cascaded as individual layers due to the computational problems that arise from the small separation of the layers.

APPENDIX A
ELECTRIC DYADIC GREEN'S FUNCTION OF THE THIRD KIND FOR THE ELECTRIC-FIELD VECTOR

The electric dyadic Green's function $\overline{\overline{G}}_{e1}(\vec{r}, \vec{r}')$ is obtained as the solution of the coupled set of vector-wave equations [8], [15]

$$
\begin{aligned}
&\nabla \times \nabla \times \overline{\overline{G}}_{e1}^{(11)}(\vec{r}, \vec{r}') - k_1^2 \overline{\overline{G}}_{e1}^{(11)}(\vec{r}, \vec{r}') \\
&\quad = \overline{\overline{I}} \delta(\vec{r} - \vec{r}'), \qquad \vec{r}, \vec{r}' \in V_1 \\
&\nabla \times \nabla \times \overline{\overline{G}}_{e1}^{(21)}(\vec{r}, \vec{r}') - k_2^2 \overline{\overline{G}}_{e1}^{(21)}(\vec{r}, \vec{r}') \\
&\quad = 0, \qquad \vec{r} \in V_2; \vec{r}' \in V_1
\end{aligned}
\tag{27}
$$

subject to two sets of boundary conditions. The first one is of the first kind on the surface of a conducting shield and ground plane at $z = \tau$, including the surface of slot apertures (Fig. 2)

$$
\hat{n} \times \overline{\overline{G}}_{e1}^{(i1)}(\vec{r}, \vec{r}') = 0, \qquad i = 1, 2.
\tag{28}
$$

The second set describes the mixed continuity conditions for the electric Green's function dyadics of the third kind on the interface of adjacent dielectric layers at $z = 0$ as follows:

$$
\begin{aligned}
\hat{z} \times \overline{\overline{G}}_{e1}^{(11)}(\vec{r}, \vec{r}') &= \hat{z} \times \overline{\overline{G}}_{e1}^{(21)}(\vec{r}, \vec{r}') \\
\hat{z} \times \left(\nabla \times \overline{\overline{G}}_{e1}^{(11)}(\vec{r}, \vec{r}') \right) &= \hat{z} \times \left(\nabla \times \overline{\overline{G}}_{e1}^{(21)}(\vec{r}, \vec{r}') \right).
\end{aligned}
\tag{29}
$$

It should be noted that the location of the δ sources in the above formulation is considered to be in the region V_1. Similarly, the boundary-value problem for the electric Green's dyadics $\overline{\overline{G}}_{e1}^{(22)}$ and $\overline{\overline{G}}_{e1}^{(12)}$ can be formulated for δ-sources positioned in the region V_2. Solution of the boundary-value problem (27)–(29) yields nine components of the electric Green's function dyadics expressed in terms of double infinite series expansions over the complete system of orthonormal eigenfunctions of the Helmholtz operator with one-dimensional z-directed scalar Green's functions

$$
\left\{ \begin{matrix} G_{ij}^{(11)} \\ G_{ij}^{(21)} \end{matrix} \right\} = \sum_{m=0}^{\infty} \sum_{n=0}^{\infty} \varphi_{mn}^i(x, y) \varphi_{mn}^j(x', y') \left\{ \begin{matrix} f_{mn,ij}^{(11)} \\ f_{mn,ij}^{(21)} \end{matrix} \right\},
$$
$$
i, j = x, y, z.
$$

A scalar form of the vector wave equation (27) for Green's function dyadics $\overline{\overline{G}}_{e1}^{(11)}$ and $\overline{\overline{G}}_{e1}^{(21)}$ is combined into three independent systems of equations. The first system of scalar equations, obtained for G_{xx}, G_{yx} and G_{zx} components of the Green's functions, is reduced to the second-order differential equations for the z-directed one-dimensional functions $f_{mn,ij}$.

Those functions are obtained as a superposition of primary and scattered parts

$$f_{mn,xx}^{(11)} = \frac{\left(k_1^2 - k_x^2\right)}{k_1^2}\frac{e^{-\gamma_1|z-z'|}}{2\gamma_1} + \alpha_1(z')e^{\gamma_1 z}$$

$$f_{mn,xx}^{(21)} = \alpha_2(z')e^{-\gamma_2 z} + \alpha_3(z')e^{\gamma_2(z-\tau)}$$

$$f_{mn,yx}^{(11)} = -\frac{k_x k_y}{k_1^2}\frac{e^{-\gamma_1|z-z'|}}{2\gamma_1} + \alpha_4(z')e^{\gamma_1 z}$$

$$f_{mn,yx}^{(21)} = \alpha_5(z')e^{-\gamma_2 z} + \alpha_6(z')e^{\gamma_2(z-\tau)}$$

$$f_{mn,zx}^{(11)} = \frac{1}{\gamma_1^2}\frac{\partial}{\partial z}\left(k_x f_{mn,xx}^{(11)} + k_y f_{mn,yx}^{(11)}\right)$$

$$f_{mn,zx}^{(21)} = \frac{1}{\gamma_2^2}\frac{\partial}{\partial z}\left(k_x f_{mn,xx}^{(21)} + k_y f_{mn,yx}^{(21)}\right). \quad (30)$$

The unknown coefficients $\alpha_p(z')$, $(p = 1, \cdots, 6)$ in (30) are obtained subject to the boundary and continuity conditions (28) and (29).

The other components of the Green's functions are derived from the second and third systems of scalar equations using a similar approach to the above for the G_{xx}, G_{yx}, and G_{zx} components.

APPENDIX B
ELECTRIC DYADIC GREEN'S FUNCTION OF THE THIRD KIND FOR THE MAGNETIC-FIELD VECTOR

Only the formulation of the boundary-value problem for dyadic Green's functions will be shown here due to the similarity of the approach to that discussed in the Appendix A. The electric dyadic Green's function $\overline{\overline{G}}_{e2}(\vec{r}, \vec{r}')$ is obtained satisfying the coupled set of vector-wave equations

$$\nabla \times \nabla \times \overline{\overline{G}}_{e2}^{(22)}(\vec{r}, \vec{r}') - k_2^2 \overline{\overline{G}}_{e2}^{(22)}(\vec{r}, \vec{r}')$$
$$= \overline{\overline{I}}\delta(\vec{r} - \vec{r}'), \qquad \vec{r}, \vec{r}' \in V_2$$
$$\nabla \times \nabla \times \overline{\overline{G}}_{e2}^{(12)}(\vec{r}, \vec{r}') - k_1^2 \overline{\overline{G}}_{e2}^{(12)}(\vec{r}, \vec{r}')$$
$$= 0, \qquad \vec{r} \in V_1; \vec{r}' \in V_2. \quad (31)$$

The boundary conditions (analogous to those for the magnetic field on the surface of a perfect conductor) on the surface of a conducting shield and ground plane at $z = \tau$, including the surface of slot apertures (Fig. 2), are

$$\hat{n} \times \nabla \times \overline{\overline{G}}_{e2}^{(i2)}(\vec{r}, \vec{r}') = 0,$$
$$\hat{n} \cdot \overline{\overline{G}}_{e2}^{(i2)}(\vec{r}, \vec{r}') = 0, \qquad i = 1, 2 \quad (32)$$

and the mixed continuity conditions for the electric Green's function dyadics of the third kind on the interface of adjacent layers at $z = 0$ (analogous to continuity conditions for tangential components of the electric and magnetic fields expressed in terms of the magnetic field vector) are

$$\hat{z} \times \overline{\overline{G}}_{e2}^{(12)}(\vec{r}, \vec{r}') = \hat{z} \times \overline{\overline{G}}_{e2}^{(22)}(\vec{r}, \vec{r}')$$
$$\frac{1}{\epsilon_1}\hat{z} \times \left(\nabla \times \overline{\overline{G}}_{e2}^{(12)}(\vec{r}, \vec{r}')\right) = \frac{1}{\epsilon_2}\hat{z} \times \left(\nabla \times \overline{\overline{G}}_{e2}^{(22)}(\vec{r}, \vec{r}')\right). \quad (33)$$

Note that the location of the δ-sources in the above formulation (31)–(33) is considered to be in the region V_2. This is necessary in order to formulate the magnetic-field integral equation in this region and to satisfy the continuity conditions on the surface of slot apertures. The boundary-value problem for the electric Green's function dyadics $\overline{\overline{G}}_{e2}^{(11)}$ and $\overline{\overline{G}}_{e2}^{(21)}$ has also been formulated for δ sources positioned in the region V_1, and the Green's functions derived have been implemented in the determination of the GSM transmission coefficient S_{12}.

APPENDIX C
ELECTRIC DYADIC GREEN'S FUNCTION OF THE SECOND KIND

The electric dyadic Green's function $\overline{\overline{G}}_{e2}^{(3)}(\vec{r}, \vec{r}')$ is obtained for a semiinfinite waveguide filled with dielectric with permittivity ϵ_3 and terminated by a ground plane at $z = \tau$. This Green's function is determined as the analog of the magnetic field vector satisfying the vector-wave equation at each interior point of the region V_3 and the magnetic-type boundary conditions on the ground plane, including the surface of slot apertures at $z = \tau$. Components of the Green's dyadic are expressed in terms of double series expansions over the complete system of eigenfunctions (shown in the Appendix A) with one-dimensional z-directed Green's functions determined in the following form:

$$f_{mn,xx}^{(3)} = \frac{\left(k_3^2 - k_x^2\right)}{2\gamma_3 k_3^2}\left[e^{-\gamma_3|z-z'|} + e^{-\gamma_3(z+z'-2\tau)}\right]$$

$$f_{mn,xy}^{(3)} = f_{mn,yx}^{(3)} = -\frac{k_x k_y}{2\gamma_3 k_3^2}\left[e^{-\gamma_3|z-z'|} + e^{-\gamma_3(z+z'-2\tau)}\right]$$

$$f_{mn,yy}^{(3)} = \frac{(k_3^2 - k_y^2)}{2\gamma_3 k_3^2}\left[e^{-\gamma_3|z-z'|} + e^{-\gamma_3(z+z'-2\tau)}\right], \quad (34)$$

Note that the transverse components of the Green's function $\overline{\overline{G}}_{e2}^{(3)}$ are primarily of interest as it appears in the scattering integral in (4). This Green's function has been also obtained in terms of rectangular vector-wave functions [12].

REFERENCES

[1] R. York and Z. Popović, Eds., *Active and Quasi-Optical Arrays for Solid-State Power Combining*. New York: Wiley, 1997.
[2] A. Mortazawi, T. Itoh, and J. Harvey, Eds., *Active Antennas and Quasi-Optical Arrays*. Piscataway, NJ: IEEE Press, 1999.
[3] L. W. Epp and R. P. Smith, "A generalized scattering matrix approach for analysis of quasi-optical grids and de-embedding of device parameters," *IEEE Trans. Microwave Theory Tech.*, vol. 44, pp. 760–769, May 1996.
[4] S. C. Bundy and Z. B. Popović, "A generalized analysis for grid oscillator design," *IEEE Trans. Microwave Theory Tech.*, vol. 42, pp. 2486–2491, Dec. 1994.
[5] A. Alexanian, N. J. Kolias, R. C. Compton, and R. A. York, "Three-dimensional FDTD analysis of quasi-optical arrays using Floquet boundary conditions and Berenger's PML," *IEEE Microwave Guided Wave Lett.*, vol. 6, pp. 138–140, Mar. 1996.
[6] A. I. Khalil and M. B. Steer, "A generalized scattering matrix method using the method of moments for electromagnetic analysis of multilayered structures in waveguide," *IEEE Trans. Microwave Theory Tech.*, vol. 47, pp. 2151–2157, Nov. 1999.
[7] R. E. Collin, *Field Theory of Guided Waves*. New York: IEEE Press, 1991.
[8] C.-T. Tai, *Dyadic Green's Functions in Electromagnetic Theory*. Piscataway, NJ: IEEE Press, 1993.
[9] L.-W. Li, P.-S. Kooi, M.-S. Leong, T.-S. Yeo, and S.-L. Ho, "Input impedance of a probe-excited semi-infinite rectangular waveguide with arbitrary multilayered loads—Part I: Dyadic Green's functions," *IEEE Trans. Microwave Theory Tech.*, vol. 43, pp. 1559–1566, July 1995.

[10] G. V. Eleftheriades, J. R. Mosig, and M. Guglielmi, "A fast integral equation technique for shielded planar circuits defined on nonuniform meshes," *IEEE Trans. Microwave Theory Tech.*, vol. 44, pp. 2293–2296, Dec. 1996.

[11] A. I. Khalil, A. B. Yakovlev, and M. B. Steer, "Efficient method-of-moments formulation for the modeling of planar conductive layers in a shielded guided-wave structure," *IEEE Trans. Microwave Theory Tech.*, vol. 47, pp. 1730–1736, Sept. 1999.

[12] L.-W. Li, P.-S. Kooi, M.-S. Leong, T.-S. Yeo, and S.-L. Ho, "On the eigenfunction expansion of electromagnetic dyadic Green's functions in rectangular cavities and waveguides," *IEEE Trans. Microwave Theory Tech.*, vol. 43, pp. 700–702, Mar. 1995.

[13] Y. Rahmat-Samii, "On the question of computation of the dyadic Green's function at the source region in waveguides and cavities," *IEEE Trans. Microwave Theory Tech.*, vol. MTT-23, pp. 762–765, Sept. 1975.

[14] C.-T. Tai and P. Rozenfeld, "Different representations of dyadic Green's functions for a rectangular cavity," *IEEE Trans. Microwave Theory Tech.*, vol. MTT-24, pp. 597–601, Sept. 1976.

[15] A. B. Gnilenko and A. B. Yakovlev, "Electric dyadic Green's functions for applications to shielded multilayered transmission line problems," *Proc. Inst. Elect. Eng.*, vol. 146, pp. 111–118, Apr. 1999.

[16] A.M. Lerer and A. G. Schuchinsky, "Full-wave analysis of three-dimensional planar structures," *IEEE Trans. Microwave Theory Tech.*, vol. 41, pp. 2002–2015, Nov. 1993.

Alexander B. Yakovlev (S'94–M'97), for photograph and biography, see this issue, p. 74.

Ahmed I. Khalil (S'97) received the B.S. (with honors) and M.S. degrees from Cairo University, Giza, Egypt, in 1992 and 1996, respectively, both in electronics and communications engineering, and is currently working toward the Ph.D. degree in electrical engineering at North Carolina State University, Raleigh.

From 1992 to 1996, he was with Cairo University as a Research and Teaching Assistant. Since 1996, he was been with North Carolina State University, where he held a Research Assistantship with the Electronics Research Laboratory, Department of Electrical and Computer Engineering. His interests include numerical modeling of microwave and millimeter-wave passive and active circuits, MMIC design, quasi-optical power combining, and waveguide discontinuities.

Mr. Khalil is a member of the honor society Phi Kappa Phi.

Chris W. Hicks (S'95) received the B.S. degree in electrical engineering from the University of South Carolina, Columbia, in 1985, the M.S. degree in electrical engineering from North Carolina A&T State University, Greensboro, in 1994, and is currently working toward the Ph.D. degree in electrical engineering at North Carolina State University, Raleigh.

In 1985, he joined the Naval Air Warfare Center Aircraft Division (NAWCAD), Patuxent River, MD. He is currently with the RF Sensors Branch, where is a member of the Analytical Computational Electromagnetic Team. He is also a Research Assistant with the Department of Electrical and Computer Engineering, Electronics Research Laboratory, North Carolina State University where he is involved in quasi-optical power combining in a dielectric slab and active waveguide power combining. His research includes microwave and millimeter-wave theory and measurement techniques, EM modeling, and phase-array antennas.

Mr. Hicks was the recipient of an NAWCAD full-time graduate fellowship in 1991 and 1997.

Amir Mortazawi (S'87–M'90), for photograph and biography, see this issue, p. 97.

Michael B. Steer (S'76–M'78–SM'90–F'99) received the B.E. and Ph.D. degrees in electrical engineering from the University of Queensland, Brisbane, Australia, in 1978 and 1983, respectively.

He is currently a Professor in the School of Electronic and Electrical Engineering, The University of Leeds, Leeds, U.K., where he holds the Chair in microwave and millimeter-wave electronics. He is also Director of the Institute of Microwaves and Photonics, The University of Leeds. Until 1996, he was the Librarian of the IBIS Consortium, which provides a forum for developing behavioral models. A converter written by his group to automatically develop behavioral models from a SPICE net list (spice2ibis) is being used throughout the digital design community. His research work has been closely tied to solving fundamental problems in modeling and implementing high-speed digital and microwave circuits. His current interests in RF and microwave design are in linearization of efficient power amplifiers, spatial power-combining systems, design of millimeter-wave- and terahertz-frequency electronic circuits, high-efficiency low-cost RF technologies for wireless applications, and computer-aided engineering of mixed digital, analog, and microwave circuits. More generally, his work is directed at global modeling of microwave and millimeter-wave systems incorporating fields, circuits, devices, thermal, and mechanical effects so that entire electronic systems can be modeled. He is involved with the development of a new paradigm for the design of spatially distributed millimeter-wave systems.

Prof. Steer is active in the IEEE Microwave Theory and Techniques Society (IEEE MTT-S). In 1997, he was Secretary of the Society and is an elected member of the Administrative Committee for the 1998–2001 term. He was the recipient of a 1987 Presidential Young Investigator Award and in 1994 and 1996, he was awarded the Bronze Medallion presented by the Army Research Office for "Outstanding Scientific Accomplishment."